

Conformational adaptation and selective adatom capturing of tetrapyrridyl-porphyrin molecules on a copper (111) surface

Willi Auwärter^{+‡}, Florian Klappenberger^{+‡}, Alexander Weber-Bargioni⁺, Agustin Schiffrin⁺, Thomas Strunskus[†], Christof Wöll[†], Yan Pennec⁺, Andreas Riemann⁺, and Johannes V. Barth⁺

Departments of Chemistry and Physics & Astronomy, University of British Columbia, Vancouver, BC V6T1Z4, Canada, and Ecole Polytechnique Fédérale de Lausanne, Institut de Physique des Nanostructures, CH-1015 Lausanne, Switzerland and Lehrstuhl für Physikalische Chemie I, Ruhr-Universität Bochum, D-44780 Bochum, Germany, and Physik Department E20, Technische Universität München, D-85748 Garching, Germany

wilhelm.auwaerter@ph.tum.de

We present a combined low-temperature scanning tunneling microscopy and near-edge X-ray-adsorption fine-structure study on the interaction of tetrapyrridyl-porphyrin (TPyP) molecules with a Cu(111) surface. A novel approach using complementary experimental data and image simulations allows to determine the adsorption geometry of TPyP on Cu(111). The molecules are centered on “bridge” sites of the substrate lattice and exhibit a strong deformation involving a saddle-shaped macrocycle distortion as well as considerable rotation and tilting of the meso-substituents. We propose a bonding mechanism based on the pyridyl-surface interaction, which mediates the molecular deformation upon adsorption. Accordingly, a functionalization by pyridyl groups opens up pathways to control the anchoring of large organic molecules on metal surfaces and tune their conformational state. Furthermore, we demonstrate that the affinity of the terminal groups for metal centers allows to selectively capture individual iron atoms at low temperature.

⁺ University of British Columbia

[‡] Ecole Polytechnique Fédérale de Lausanne

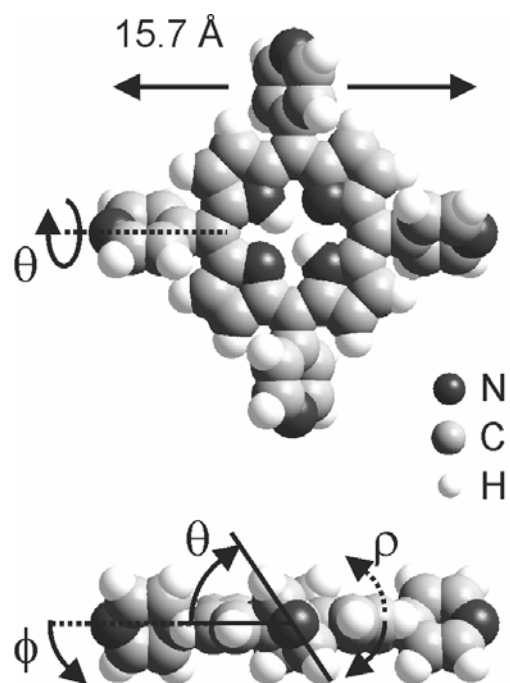
^{*} Technische Universität München

[†] Ruhr Universität Bochum

1. Introduction

The control of large functional molecules at metallic substrates is of great interest and plays a central role in various fields in science and technology, ranging from heterogeneous catalysis^{1,2} to molecular electronics³, optoelectronics⁴ based on organic thin films⁵, or single molecule contacts⁶⁻⁸. The surface chemical bonding steers the mobility of the adsorbed molecular building blocks⁹, which is decisive for a controlled self-assembly of functional architectures on the nanoscale¹⁰. Furthermore the interaction of complex molecules exhibiting internal degrees of freedom with the substrate frequently induces modifications of the molecular configuration, be it a conformational adaptation or a change in the chemical composition or electronic structure^{11,12}. These effects are reflected in a varied chemical reactivity, induced charge transfer or altered magnetic properties¹³. Thus it is of fundamental interest to determine the adsorption geometry, i.e. the internal conformation as well as the adsorption site of the molecule on the substrate atomic lattice. This set of information allows to categorize adsorbate-substrate interactions and yields a basis for a theoretical discussions of important issues as bonding mechanisms, bond energies, electronic level alignment or functional properties based on conformational or supramolecular design.

Because of its excellent real space imaging capabilities Scanning Tunneling Microscopy (STM) is ideally suited to observe, characterize and manipulate individual molecules on conducting substrates. Notably the conformation¹⁴⁻¹⁶, mobility¹⁷⁻²² and self-assembly²³⁻²⁵ of porphyrin species on metal surfaces attracted considerable interest in recent years. This class of molecules exhibits an intriguing variety of functional properties, which are exploited in both biological and artificial systems^{26,27}. Accordingly, these versatile molecules are promising building blocks to assemble functional nanostructures on surfaces, specifically opening up new opportunities to build sensors and nanoscale optical and magnetic materials^{28,29}. In the context of this article it is relevant to mention two features connected to the functionality of porphyrins. The rotational degrees of freedom of the chosen meso-substituents and the flexibility of the porphyrin macrocycle allow for a conformational adaptation of the molecule to its local environment. Relative to the molecular core, the conformation of the leg is determined by two angles (θ and ϕ), which are indicated in Scheme 1. The angle θ describes the rotation of a pyridyl group around the C-C bond connecting it to the porphyrin core, while ϕ indicates a bending of this C-C bond out of the macrocycle plane¹⁵. To some extent, the dihedral angle θ and the nonplanar deformation (ρ) of the macrocycle are interconnected through steric repulsion between hydrogen atoms of the ring and the hydrogens of the porphyrin macrocycle. Accordingly, many reports on macrocycle distortions as well as varying dihedral angles are available for solid state phases³⁰⁻³⁴. On surfaces however, the vast majority of studies focuses solely on the orientation^{14,15,25} and considerate manipulation^{35,36} of the meso-substituents. Only some recent reports speculate on nonplanar adsorption geometries^{13,16,37,38}, however by pure STM imaging the question of intramolecular structure cannot be quantitatively addressed.



Scheme 1 Model of an isolated tetrapyrrolyl-porphyrin (TPyP) molecule in its groundstate conformation. The top view (upper panel) highlights the central porphyrin core and the four terminal pyridyl groups, the legs. In the side view (lower panel) we indicate the two angles (θ and ϕ), which determine the conformation of the legs relative to the porphyrin macrocycle. A possible nonplanar deformation of the latter is described by the angle ρ .

Meso-substituted porphyrins with a wide variety of endgroups can be synthesized. This provides a series of building blocks for metal-organic networks in solid state chemistry^{39,40}. Specifically tetraarylporphyrins functionalized by pyridyl substituents interact via the terminal nitrogen lone pair with a wide variety of reactive metal centers ($\text{Cu}^{41,42}$, Fe^{43} , Pd^{44} , Pb^{45}) to form ordered structures. By contrast, on surfaces, the pyridyl mediated interaction of porphyrins with the substrate or coadsorbed atoms was not explored to date. Nevertheless, the considerate choice of substituents with specific chemical or electrostatic characteristics allows to tune the adsorbate-adsorbate interaction⁴⁶, and thus to assemble not only supramolecular aggregates with controlled size and shape⁴⁷ but also nanoporous host networks^{48,49}.

Here, we focus on the detailed understanding and control of adsorbate-substrate interactions. By employing a nitrogen termination, it is possible to anchor tetrapyrrolylporphyrin (TPyP) on the smooth Cu(111) surface and to inhibit molecular diffusion even at room temperature. The underlying binding mechanism locks the molecule into specific positions on the substrate lattice and induces a considerable deformation of TPyP. A saddle-shape conformational adaptation is determined by STM in combination with image simulations and near-edge X-ray adsorption fine-

structure (NEXAFS) measurements. Additionally, we directly monitor the affinity of metal centers to the pyridyl groups by selectively attaching Fe adatoms to the TPyP moieties.

2. Experimental Section

All scanning tunneling microscope (STM) experiments were performed in a custom-designed ultrahigh vacuum (UHV) apparatus comprising a commercial low-temperature STM⁵⁰ based on a design described in ref [51]. The system base pressure is below 2×10^{-10} mbar.

The Cu(111) single crystal surface was cleaned by repeated cycles of Ar⁺ sputtering (800 eV) followed by annealing to 780 K. Subsequently, TPyP (97+% purity, Frontier Scientific) was deposited by organic molecular beam epitaxy (OMBE) from a quartz crucible held at 525 K. Typical evaporation rates are roughly 0.03 monolayer/min (one monolayer corresponds a densely packed molecular film). TPyP was thoroughly degassed prior to any experiments resulting in a background pressure in the 10^{-10} mbar range during deposition. After dosing TPyP at room temperature, the sample was cooled down and transferred into the STM, where constant current images were recorded at about 11 K using electrochemically etched tungsten tips. In the figure captions *V* refers to the bias voltage applied to the sample.

High-purity carbon monoxide (CO) gas was dosed in-situ at sample temperatures not exceeding 18 K. Fe atoms were evaporated from a home-made water-cooled cell by resistively heating a W filament surrounded by a Fe wire of high purity (99.998%). Our experimental setup allows direct access of the atomic beam to the sample placed in the STM.

The NEXAFS data were taken at the HE-SGM beamline at BESSY II in Berlin. For the measurements at the N K edge the partial electron yield mode (retarding voltage 270 V) was used. The energy resolution was approximately 0.5 eV. All spectra have been referenced against a characteristic peak (399 eV) in simultaneously recorded spectra of a contaminated Au grid. For each incidence angle an average of four spectra is presented. To concentrate on the information related to the TPyP adsorbate layer, we processed the raw data by subtracting the signal of the bare crystal, then corrected for the transmission through the beamline and finally normalized the edge jump to one.

As a basis to corroborate and analyze the experimental structural data, we applied basic molecular mechanics calculations to optimize the geometry of TPyP moieties. Specifically, the MM+ force field of the Hyperchem 7.5 molecular modeling package⁵² was used to calculate and minimize the total energy of the system.

The STM image simulations are based on semiempirical extended Hückel calculations⁵². A constant electron density contour is obtained by integrating over the relevant molecular orbitals, which mimics a constant current STM image⁵³. This procedure proved to reliably reproduce the appearance of adsorbed molecules^{54,55}, including TPyP on the Ag(111) surface²⁵.

3. Results and Discussion

A. Molecular appearance and adsorption site

Figure 1a shows a large scale STM image of two Cu(111) terraces after submonolayer deposition of TPyP at 300 K. Isolated bright spots, which are randomly distributed on the surface, are clearly discernible. High-resolution data as displayed in Figure 1b reveal that each of these protrusions corresponds to a single TPyP molecule, whereby only one species is observed. The findings that TPyP neither self assembles into highly ordered agglomerates nor considerably decorates the step edges, signals appreciable interaction between the molecule and the Cu(111) surface. This restricts the mobility of TPyP on Cu(111), in marked contrast to the adsorption of the very same molecule on the less reactive Ag(111) surface, where extended islands are formed even well below room temperature²⁵. Nevertheless, the individual TPyP molecules align along the close-packed $\langle 110 \rangle$ high-symmetry directions of the Cu(111) substrate, as inferred by imaging the atomic lattice (see Figure 1c). Thus, three possible azimuthal orientations of TPyP on Cu(111) exist, which are all observed in the experimental data. Discussing the rotational ordering of molecules on surfaces implies that the adsorbates reveal an apparent symmetry break. Indeed STM images with intramolecular resolution (cf. Figure 1b) allow defining a symmetry axis running through the two bright protrusions close to the center of the molecule. Besides these two prominent maxima, one can identify four broad lobes. From the molecular dimensions (side length ~ 12 Å), we assign each lobe to one of the pyridyl legs. The overall appearance of TPyP on Cu(111) thus strongly deviates from the one observed on Ag(111), which is imaged with a rectangular envelope and a depression in the center²⁵. As in the latter case the molecule proved to be very close to its natural gas phase configuration (compare Scheme 1), the topographic appearance on Cu(111) points to a strong distortion of TPyP and thus to an adsorption induced modification of the molecular conformation.

Before addressing this issue in more detail, we discuss the adsorption site of TPyP on Cu(111). The observation of individual molecules azimuthally oriented along substrate high-symmetry directions indicates that TPyP is located at specific sites of the underlying Cu(111) lattice. However, as the positioning can have a drastic impact on STM images of molecules on surfaces⁵⁶, it is important to verify this assumption and to determine the adsorption site, prior to any further discussion on the molecular conformation.

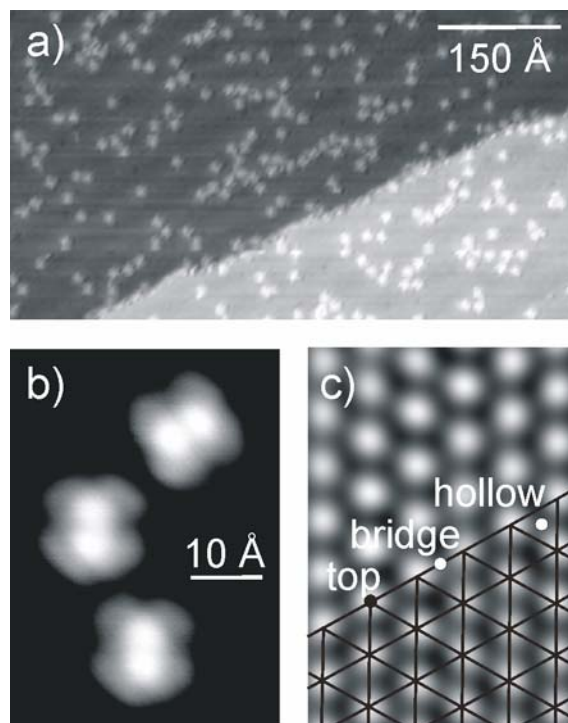


Figure 1 TPyP adsorption on Cu(111) at room temperature: a) large scale STM topograph depicting a random distribution of TPyP molecules on the Cu terraces ($V=-1.1V$, $I=0.17nA$). b) high resolution STM image revealing intramolecular features ($V=-0.5V$, $I=0.35nA$). c) the Cu(111) atomic lattice. High symmetry adsorption sites are marked. ($V=27mV$, $I=0.65nA$).

Due to incompatible imaging parameters, it is not possible to simultaneously resolve the substrate lattice and the adsorbed TPyP molecule. As an alternative solution, we applied coadsorbed CO molecules as markers to determine the adsorption site of TPyP. Related approaches were successfully used to obtain the adsorption site of adatoms and molecules⁵⁷⁻⁶⁰. It is well known that at low coverage CO molecules stand upright and occupy exclusively “on top” positions on the Cu(111) lattice^{61,62}. Additionally, TPyP and CO molecules can easily be imaged simultaneously by STM. This is illustrated in Figure 2a: after a minute exposure to CO, dosed in-situ at a sample temperature of 18 K, dim sombrero shaped protrusions representing single CO molecules are visible in between the TPyP molecules. By matching a hexagonal grid representing the Cu(111) lattice (compare Figure 1d) with the positions of the CO molecules, one can conclude that the TPyP molecules are centered on “bridge” sites, irrespective of which of the three azimuthal orientations they follow (cf. Figure 2). The dissimilar appearance of the legs is tentatively explained by partial CO attachment and height modulations due to surface state scattering.

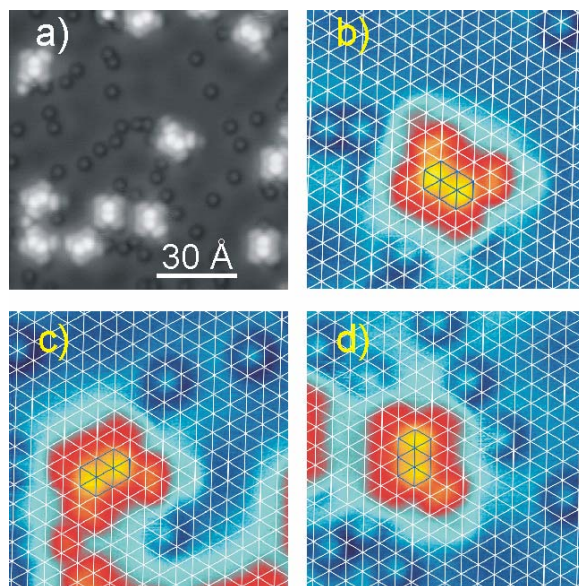


Figure 2 Adsorption site determination of TPyP on Cu(111) by using CO molecules as markers. The top left panel demonstrates the simultaneous imaging of CO and TPyP. The three color-coded plots show that TPyP is centered on bridge site of the underlying Cu(111) lattice (compare Figure 1c), irrespective of the azimuthal orientation ($V=250\text{mV}$, $I=0.2\text{nA}$).

B. Molecular conformation

We succeeded to determine the molecular conformation of TPyP on Cu(111) by the use of a novel procedure based on two steps. First we apply NEXAFS measurements, which yield information on the dihedral angles between the molecular π systems and the surface plane. Subsequently we refine the NEXAFS results by comparing simulated STM images with the experimental high-resolution data. The nitrogen K edge of a monolayer of TPyP on Cu(111) (Figure 3) exhibits a pronounced dichroism which differs remarkably from that of a multilayer of the same molecule (not shown) indicating a strong conformational adaptation. The spectra are dominated by 2 peaks in the π^* region (399.4 eV and 400.9 eV) and a broad σ^* structure. For the analysis we need to decompose the spectra in parts stemming from the different types of N. To this end we focus on the π^* range, as the broad σ^* features prohibit a reliable analysis. Based on earlier reports⁶³⁻⁶⁶ we expect several overlapping resonances in the π^* range (397 eV – 405 eV), namely two from the pyridil legs and three from each of the two macrocycle nitrogens. Fitting this range with gauss-shaped peaks combined into three sets where each set was optimized to reproduce published reference spectra yields a reasonable agreement with the experimental data and allows to determine the angular dependence of each of the resonances. It becomes evident that the first peak at 399.4 eV and the second at 400.9 eV are mainly due to the pyridilic N and the macrocycle N absorption, respectively. Clearly the two peaks behave differently when changing the photon beam incidence from grazing (30° , dotted curve) to normal (90° , solid curve), signifying different orientation of the according molecular moieties (Figure 3, inset). It follows that the average of the normals on the pyridil endgroups has an angle of 30° (inset, solid

line) with the substrate. For the average of the normals on the pyrrol groups of the macrocycle a value of 50° is found.

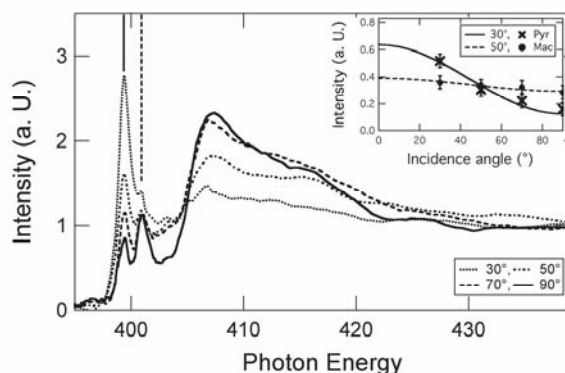


Figure 3 Nitrogen K edge spectra (NEXAFS) of one monolayer TPyP on Cu(111) exhibiting strong dichroism. Two main peaks related to different molecular moieties are marked by vertical lines. Their angular dependence (see inset) yields a nonplanar macrocycle (50°) and inclined pyridyl groups (30°).

These findings indicate marked distortions of TPyP upon adsorption, in line with the STM observations (cf. Figure 1b). However it is important to realize that the two values determined by NEXAFS do not allow for an unequivocal determination of all three important intramolecular angles, and thus the geometry of the molecule. This is easily recognized by discussing the conformation of the pyridyl legs relative to the porphyrin macrocycle⁶⁷, which is defined by the two angles θ and ϕ introduced before (cf. Scheme 1). NEXAFS however only yields the inclination angle between the pyridyl group and the surface. Thus, there are many possible combinations of θ and ϕ angles, which are consistent with the single value given by NEXAFS.

To resolve the molecular conformation despite this limitation, we simulated STM images for a set of geometries (c.f. Figure 4a-c), which are compatible with the NEXAFS data, and compared them to a typical experimental image (see Figure 4d). This scan was recorded at a low negative sample bias voltage, thus representing occupied electronic states. Accordingly, all the simulated STM images presented below are based on the density of states of the highest occupied molecular orbitals (HOMO and HOMO-1)⁶⁸. Figure 4a shows a simulated STM image of TPyP. It represents a geometry, which was obtained by reducing the dihedral angle θ to 30° while keeping the C-C bond parallel to the surface ($\phi=0$). This pyridyl conformation goes in hand in hand with a saddle-shaped distortion of the molecular core³¹: the pyrrole rings are fixed at a tilt angle ρ of 45° . The simulated image is dominated by two longish protrusions, which extend to the far ends of the molecule. Obviously, this contour bears no close resemblance to the experimental STM image presented in Figure 4d. The poor agreement between calculated and simulated STM topographs allows to discard this molecular conformation and compels us to consider a bending of the C-C bond out of the macrocycle plane.

Accordingly, we freeze the pyridyl conformation by setting the angles to $\theta=20^\circ$ and $\phi=10^\circ$ and apply a macrocycle distortion ρ of 35° . The resulting simulated image (Figure 2b) is in good agreement with the experimental data. Both the two central maxima and the appearance of the legs are reproduced. Furthermore, one can distinguish two different types of indentations along and perpendicular to the molecular axis, respectively.

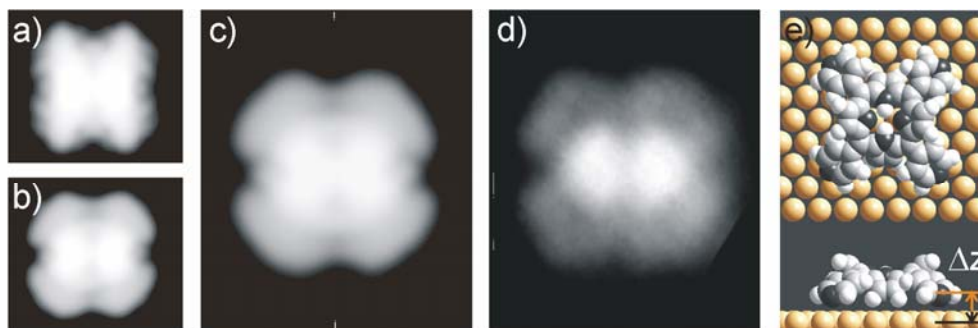


Figure 4 Comparison of simulated STM images based on molecular geometries compatible with the NEXAFS results (a-c) with an experimental STM topograph (d) ($V=-0.5V$, $I=0.15nA$). e) Adsorption geometry of TPyP on Cu(111). Top view (top) and side view (bottom) clearly reveal the molecular distortion, i.e. a saddle-shaped macrocycle deformation as well as flexure of the pyridyl moieties, upon adsorption.

Finally, Figure 4c shows the simulated STM image for a slightly varied geometry ($\theta=0^\circ$, $\phi=30^\circ$, $\rho=45^\circ$). Considering the simplicity of the applied procedure, the agreement between experiment and calculations is striking. Not only is the molecular outline nicely reproduced, but also the positions of the two central maxima improved in comparison to Figure 4b. In addition, the macrocycle distortion ρ resulting from this optimized geometry is in good agreement with the value of 50° determined by NEXAFS (the saddle-shape and in particular the angle ρ Figure 4b and c are based on, are obtained by optimizing the geometry of the porphyrin macrocycle by the MM+ procedure complying with the constraints given by the pyridyl conformation).

In summary, a molecular conformation characterized by pyridyl rings, which are heavily rotated around the C-C bond ($\theta \leq 10^\circ$) and additionally bent towards the substrate ($20^\circ \leq \phi \leq 30^\circ$) inducing a saddle-shaped macrocycle distortion ($40^\circ \leq \rho \leq 50^\circ$), describes the experimental results best.

Already knowing the adsorption site, we thus can establish a complete model for the adsorption geometry of TPyP on Cu(111), which is depicted in Figure 4e. To our knowledge, this is one of very few examples where STM and complementary techniques allowed to determine the full adsorption geometry of a large functional molecule, i.e. conformation and adsorption site. Furthermore, total energy calculations in the MM+ framework indicate that the pyridyl nitrogens are separated by about 2.5 \AA (Δz) from the surface plane defined by the atomic centers. The distance of the pyrrole nitrogens from the substrate is considerably larger.

Now we briefly address the possible reasons for the strong deformation of TPyP upon adsorption on Cu(111). An inspection of Figure 4e reveals that there are two groups of atoms closest to the surface: the pyridyl nitrogens and the outer pyrrolic hydrogens. Judging from the high affinity of the nitrogen to metals discussed in the introduction, the attractive N-Cu interaction is most likely the trigger for the deformation. A close distance between pyridilic N and the Cu surface atoms can only be achieved for small dihedral angles θ and a tilt of the pyridyl leg towards the substrate. As a result, the marked distortion of the porphyrin macrocycle is induced by steric constraints as a consequence of the bending of the legs.

At this point it is instructive to further discuss two issues. We already mentioned the strikingly different adsorption behaviour of TPyP on Ag(111) and Cu(111). These differences can be rationalized by comparing the interactions between pyridyl molecules and Ag or Cu surfaces, respectively. Indeed the bonding of pyridyl to Cu via the N lone pair proved to be very important, while in the case of Ag(111) the interaction with the π electrons of the aromatic ring is dominant⁶⁹. At low coverage, this difference results in pyridyl standing upright on Cu(110) with the N pointing towards the surface^{70,71}, while it prefers a rather planar adsorption geometry on Ag(111)^{72,73}.

A second comparison also corroborates the importance of the nitrogen for the reported adsorption behaviour. Co-Tetraphenylporphyrin (Co-TPP) is a molecule closely related to TPyP. However, it is terminated by phenyl rings and the macrocycle hosts a Co ion bonded to the four pyrrolic nitrogens. After room temperature deposition of Co-TPP on Cu(111) we observe highly ordered compact islands of Co-TPP. Evidencing that the room temperature mobility of Co-TPP is higher than for TPyP, despite the additional interaction of the Co center with the metal substrate. Consequently, also this observation points to the decisive role the nitrogen lone pairs play for the mobility and conformation of TPyP on Cu(111).

C. Reactivity towards metal centers

A second type of bonding mechanism between the terminal pyridyl groups and metal atoms is revealed by the experiment presented in Figure 5. Single Fe atoms were added in-situ at 8 K, where thermal diffusion is frozen in. Figure 5a accordingly shows randomly distributed Fe monomers appearing as round protrusions coexisting with TPyP molecules. In a next step the sample temperature was slightly increased to about 15 K, which allows the Fe adatoms to freely migrate on the surface, while the TPyP is immobile. Subsequently, the sample was cooled down again to freeze the adatom motion. As a result Fe is selectively captured by the pyridyl groups (Figure 5b). Once attached the adatoms stick and do not diffuse. The modified imaging characteristics of both Fe and TPyP-endgroups indicate marked chemical interaction, and differ in this respect from the previously reported STM data of 2D Cu- and Fe-carboxylate mononuclear compounds^{74,75} or dinuclear nanogrids^{76,77}. Judging from the unchanged appearance of the molecular core a relaxation of the TPyP is rather unlikely.

Analogously to the determination of the TPyP adsorption site, we address in Figure 5c and d the Fe positions by overlaying an atomic lattice. We find that the “bridge” adsorption site of TPyP is consistent with isolated Fe adatoms occupying “hollow” sites of the underlying substrate atomic lattice (Figure 5c), an adsorption site suggested in previous reports⁷⁸. The convolution of the molecular and atomic signatures hampers a precise and reliable determination of the positions of the Fe centers in the TPyP-Fe complexes. Nevertheless, the STM image in Figure 5d demonstrates the highly symmetric appearance and directionality of the pyridyl-Fe complex and suggests a lateral Fe-N distance of about 2.4 ± 0.5 Å. This value compares well with a Fe-pyridyl bond length of 2.2 Å reported for a three dimensional Fe-porphyrin complex⁴² and the positioning of diiron units simultaneously coordinated by carboxylate and pyridil ligands on Cu(100)⁷⁹.

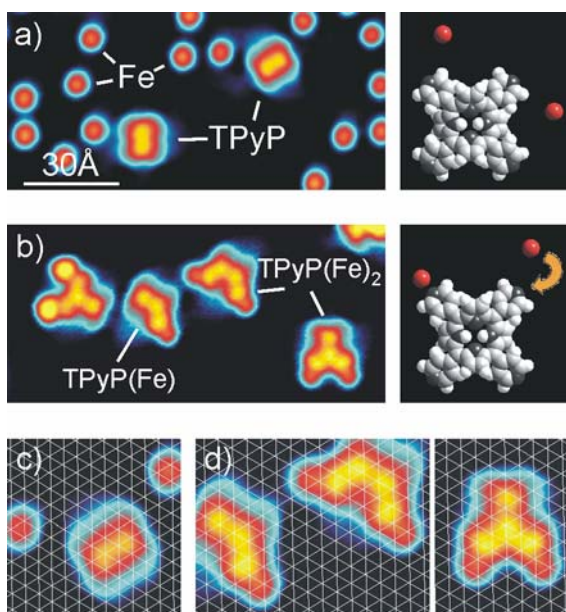


Figure 5 Selective attachment of Fe adatoms to the pyridyl groups of TPyP (a,b, a: $V=30$ mV, $I=0.2$ nA, b: $V=20$ mV, $I=0.2$ nA). See text for discussion. To main steps of this experiment are schematically illustrated in the column on the right. c) a detailed view of a) which indicates that the reported TPyP adsorption site is consistent with single Fe atoms centered on hollow sites. d) the overlaid substrate lattice grid exemplifies the highly symmetric appearance of the TPyP(Fe)_n complexes.

These findings confirm that the N containing ligands retain their affinity towards metal centers despite the conformational adaptation implying a non-planar orientation of pyridil groups, and directly visualize the impact of metal-ligand interactions on a metallosupramolecular self-assembly process in two dimensions where the ligands are spatially anchored. Furthermore additional incoming Fe monomers can be trapped by the metal-ligand complex, resulting in small metal clusters pinned to the pyridyl groups of the TPyP. This approach allows in principle to self-assemble large quantities of metal-molecule-metal bridges⁸⁰ which might prove very interesting to study metal-molecule contacts as these junctions are defined on an atomic level⁶.

4. Conclusions

The presented experiments indicate that the attractive interactions between the functional pyridyl moieties and the Cu substrate, presumably mediated by the lone pair electrons of nitrogen, not only immobilize the TPyP molecule up to room temperature, but also promote a strong deformation of the molecular geometry. Furthermore the functional pyridyl legs are strong attractors for Fe atoms. This permitted to present snapshots of the self-assembly process of a metal-organic complex in two dimensions.

Our findings allow to selectively attach metal centers to pyridyl moieties, and open up pathways to steer the mobility of large organic molecules. Especially the possibility to immobilize functional species on surfaces even at elevated temperature should facilitate the controlled construction of complex molecular architectures on surfaces.

In addition we presented a novel approach to determine the geometry of adsorbed molecules. Combining the well established NEXAFS method with a procedure relating STM simulations to high-resolution data, presents a useful tool to study conformations of large molecular adsorbates, which should be applicable for a wide variety of systems. Therewith, we quantified for the first time the saddle-shaped geometry of an adsorbed free-base porphyrin molecule. Such structural information provides a prerequisite to control functional properties of adsorbed complex molecules and the conformational design of flexible species embedded in molecular nanoarchitectures at surfaces.

Acknowledgements

Work supported by Canada Foundation of Innovation (CFI), National Science and Engineering research Council of Canada (NSERC), British Columbia Knowledge Development Fund (BCKDF) and the European Union BIOMACH project. W.A. thanks the Swiss National Science Foundation (SNF) and A.W.-B. the German Academic Exchange Service (DAAD) for financial support. Support of the travel of T.S. to the Berlin synchrotron source by the BMBF through project # 05 ES3XBA/5 is gratefully acknowledged.

References

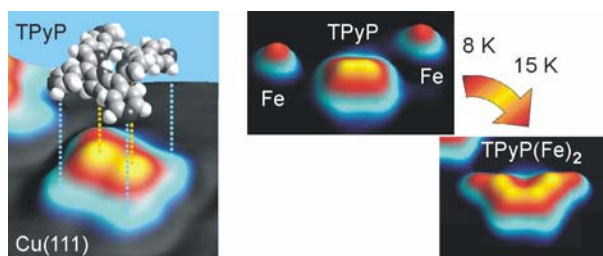
- (1) Castonguay, M.; Roy, J.-R.; Rochefort, A.; McBreen, P. H. *J. Am. Chem. Soc.* **2000**, *122*, 518-524.
- (2) Barlow, S. M.; Raval, R. *Surf. Sci. Rep.* **2003**, *50*, 201-341.
- (3) Joachim, C.; Gimzewski, J. K.; Aviram, A. *Nature* **2000**, *408*, 541-548.
- (4) Forrest, S. R. *Chem. Rev.* **1997**, *97*, 1793-1896.
- (5) Ishii, H.; Sugiyama, K.; Ito, E.; Seki, K. *Adv. Mater.* **1999**, *11*, 605-625.
- (6) Nazin, G. V.; Qiu, X. H.; W.Ho *Science* **2003**, 77-81.

- (7) Moresco, F.; Gross, L.; Alemani, M.; Rieder, K.-H.; Tang, H.; Gourdon, A.; Joachim, C. *Phys. Rev. Lett.* **2003**, *91*, 036601-036604.
- (8) Grill, L.; Rieder, K.-H.; Moresco, F.; Stojkovic, S.; Gourdon, A.; Joachim, C. *Nano Letters* **2005**, 859-863.
- (9) Schunack, M.; Linderoth, T. R.; Rosei, F.; Laegsgaard, E.; Stensgaard, I.; Besenbacher, F. *Phys. Rev. Lett.* **2002**, *88*, 156102-156101-156104.
- (10) Barth, J. V.; Costantini, G.; Kern, K. *Nature* **2005**, *437*, 671-679.
- (11) Rosei, F.; Schunack, M.; Naitoh, Y.; Jiang, P.; Gourdon, A.; Laegsgaard, E.; Stensgaard, I.; Joachim, C.; Besenbacher, F. *Prog. Surf. Sci.* **2003**, *71*, 95-146.
- (12) Hauschild, A.; Karki, K.; Cowie, B. C. C.; Rohlfing, M.; Tautz, F. S.; Sokolowski, M. *Phys. Rev. Lett.* **2005**, *94*, 036106-036101-036104.
- (13) Iancu, V.; Deshpande, A.; Hla, S.-W. *Nano Lett.* **2006**, *6*, 820-823.
- (14) Jung, T. A.; Schlittler, R. R.; Gimewski, J. K. *Nature* **1997**, *386*, 696.
- (15) Moresco, F.; Meyer, G.; Rieder, K.-H.; Ping, J.; Tang, H.; Joachim, C. *Surf. Sci.* **2002**, *499*, 94-102.
- (16) Yokoyama, T.; Yokoyama, S.; Kamikado, T.; Mashiko, S. *J. Chem. Phys.* **2001**, *115*, 3814.
- (17) Ogaki, K.; Batina, N.; Kunitake, M.; Itaya, K. *J. Phys. Chem.* **1995**, *100*, 7185-7190.
- (18) Kunitake, M.; Akiba, U.; Batina, N.; Itaya, K. *Langmuir* **1997**, *13*, 1607-1615.
- (19) Shimada, T.; Hashimoto, R.; Koide, J.; Kamimuta, Y.; Koma, A. *Surf. Sci.* **2000**, *470*, L52-L56.
- (20) He, Y.; Ye, T.; Borguet, E. *J. Am. Chem. Soc.* **2002**, *124*, 11964-11970.
- (21) Suto, K.; Yoshimoto, S.; Itaya, K. *Langmuir* **2006**, *22*, 10766-10776.
- (22) Suzuki, H.; Berner, S.; Brunner, M.; Yanagi, H.; Schlettwein, D.; Jung, T. A.; Güntherodt, H.-J. *Thin Solid Films* **2001**, *393*, 325-328.
- (23) Scudiero, L.; Barlow, D. E.; Hipps, K. W. *J. Phys. Chem. B* **2000**, *104*, 11899-11905.
- (24) Scudiero, L.; Hipps, K. W.; Barlow, D. E. *J. Phys. Chem. B* **2003**, *107*, 2903-2909.
- (25) Auwärter, W.; Weber-Bargioni, A.; Riemann, A.; Schiffrin, A.; Groening, O.; Fasel, R.; Barth, J. V. *J. Chem. Phys.* **2006**, *124*, 194708.
- (26) *The Porphyrins*; Dolphin, D., Ed.; Academic: New York, 1978.
- (27) Milgrom, L. R. *The Colours of Life : An Introduction to the Chemistry of Porphyrins and Related Compounds*; Oxford University Press, 1997.
- (28) *The Porphyrin Handbook Vol6, Applications: Past, Present and Future*; Kadish, K. M.; Schmith, K. M.; Guillard, R., Eds.; Academic Press: San Diego, 2000; Vol. 6.
- (29) Elemans, J. A. A. W.; Hameren, R. v.; Nolte, R. J. M.; Rowan, A. E. *Adv. Mater.* **2006**, *18*, 1251-1266.

- (30) Pan, L.; Kelly, S.; Huang, X.; Li, J. *Chem. Commun.* **2002**, 2334-2335.
- (31) Shelnut, J. A.; Song, X.-Z.; Ma, J. G.; Jia, S.-L.; Jentzen, W.; Medforth, C. J. *Chemical Society Reviews* **1998**, *27*, 31-41.
- (32) Marques, H. M.; Brown, K. L. *Coord. Chem. Rev.* **2002**, *225*, 123-158.
- (33) Fleischer, E. B.; Miller, C. K.; Webb, L. E. *J. Am. Chem. Soc.* **1964**, *86*, 2342-2347.
- (34) Silvers, S. J.; Tulinsky, A. *J. Am. Chem. Soc.* **1967**, *89*, 3331-3337.
- (35) Moresco, F.; Meyer, G.; Rieder, K.-H.; Tang, H.; Gourdon, A.; Joachim, C. *Phys. Rev. Lett.* **2001**, *86*, 672-675.
- (36) Loppacher, C.; Guggisberg, M.; Pfeiffer, O.; Meyer, E.; Bammerlin, M.; Luthi, R.; Schlittler, R.; Gimzewski, J. K.; Tang, H.; Joachim, C. *Phys. Rev. Lett.* **2003**, *90*, 066107.
- (37) Qiu, X. H.; Nazin, G. V.; Ho, W. *Phys. Rev. Lett.* **2004**, *93*, 196806.
- (38) Auwärter, W.; Weber-Bargioni, A.; Brink, S.; Riemann, A.; Schiffrin, A.; Ruben, M.; Barth, J. V. *ChemPhysChem* **2006**.
- (39) Fujita, M. *Chem. Soc. Rev.* **1998**, *27*, 417-425.
- (40) Kosal, M. E.; Suslick, K. S. *J. Solid State Chem.* **2000**, *152*, 87.
- (41) Abrahams, B. F.; Hoskins, B. F.; Michail, D. M.; Robson, R. *Nature* **1994**, *369*, 727-729.
- (42) Hagrman, D.; Hagrman, P. J.; Zubieta, J. *Angew. Chem. Int. Ed.* **1999**, *38*, 3165-3168.
- (43) Pan, L.; Kelly, S.; Huang, X.; Li, J. *Chem. Commun.* **2002**, 2334-2335.
- (44) Drain, C. M.; Nifiatis, F.; Vasenko, A.; Batteas, J. D. *Angew. Chem. Int. Ed.* **1998**, *37*, 2344-2347.
- (45) Sharma, C. V. K.; Broker, G. A.; Huddleston, J. G.; Baldwin, J. W.; Metzger, R. M.; Rogers, R. D. *J. Am. Chem. Soc.* **1999**, *121*, 1137-1144.
- (46) Lei, S. B.; Wang, C.; Yin, S. X.; Wang, H. N.; Xi, F.; Liu, H. W.; Xu, B.; Wan, L. J.; Bai, C. L. *J. Phys. Chem. B* **2001**, *105*, 10838-10841.
- (47) Yokoyama, T.; Yokoyama, S.; Kamikado, T.; Okuno, Y.; Mashiko, S. *Nature* **2001**, *413*, 619 - 621.
- (48) Spillmann, H.; Kiebele, A.; Jung, T. A.; Bonifazi, D.; Cheng, F.; Diederich, F. *Adv. Mater.* **2006**, *18*, 275-279.
- (49) Kiebele, A.; Bonifazi, D.; Cheng, F.; Stöhr, M.; Diederich, F.; Jung, T.; Spillmann, H. *ChemPhysChem* **2006**, *7*, 1462-1470.
- (50) Createc GMBH, D-74391 Erligheim, Germany.
- (51) Meyer, G. *Review of Scientific Instruments* **1996**, 2960-2965.
- (52) HYPERCHEM; Hypercube Inc.: 1115 NW 4th street, Gainesville, Florida 32601.
- (53) Gröning, O.; Fasel, R.; EMPA Materials Science and Technology: Switzerland, 2004.

- (54) Fasel, R.; Parschau, M.; Ernst, K.-H. *Nature* **2006**, *439*, 449-452.
- (55) Fasel, R.; Parschau, M.; Ernst, K. H. *Angew. Chem. Int. Ed.* **2003**, *42*, 5178-5181.
- (56) Weiss, P. S.; Eigler, D. M. *Phys. Rev. Lett.* **1993**, *71*, 3139-3142.
- (57) Meyer, G.; Zöphel, S.; Rieder, K. H. *Phys. Rev. Lett.* **1996**, *77*, 2113-2116.
- (58) Repp, J.; Meyer, G.; Stojkovic, S. M.; Gourdon, A.; Joachim, C. *Phys. Rev. Lett.* **2005**, *94*, 026803.
- (59) Böhringer, M.; Schneider, W.-D.; Glöckler, K.; Umbach, E.; Berndt, R. *Surf. Sci.* **1998**, *419*, L95-L99.
- (60) Ohara, M.; Kim, Y.; Kawai, M. *Jpn. J. Appl. Phys.* **2005**, *44*, 5390-5392.
- (61) Ishi, S.; Ohno, Y.; Viswanathan, B. *Surf. Sci.* **1985**, *161*, 349-372.
- (62) Raval, R.; Parker, S. F.; Pemble, M. E.; Hollins, P.; Pritchard, J.; Chesters, M. A. *Surf. Sci.* **1988**, *203*, 353-377.
- (63) Jong, M. P. d.; Friedlein, R.; Sorensen, S. L.; Öhrwall, G.; Osikowicz, W.; Tengsted, C.; Jönsson, S. K. M.; Fahlman, M.; Salaneck, W. R. *Phys. Rev. B* **2005**, *72*, 035448-035441-035448.
- (64) Cudia, C. C.; Vilmercati, P.; Larciprete, R.; Cepek, C.; Zampiere, G.; Sangaletti, L.; Pagliara, S.; Verdini, A.; Cossaro, A.; Floreano, L.; Morgante, A.; Petaccia, L.; Lizzit, S.; Battocchio, C.; Polzonietti, G.; Goldoni, A. *Surf. Sci.* **2006**, *600*, 4013-4017.
- (65) Kolczewski, C.; Püttner, R.; Plashkevych, O.; Ågren, H.; Staemmler, V.; Martins, M.; Snell, G.; Schlachter, A. S.; Sant'Anna, M.; Kaindl, G.; Pettersson, L. G. M. *J. Chem. Phys.* **2001**, *115*, 6426-6437.
- (66) Hövel, S.; Kolczewski, C.; Wühn, M.; Albers, J.; Weiss, K.; Staemmler, V.; Wöll, C. *J. Chem. Phys.* **2000**, *112*, 3909-3916.
- (67) Here the macrocycle plane is defined by the four meso-carbon atoms. This description holds also in case of a saddle shaped distortion of the porphyrin core.
- (68) Including lower lying occupied molecular orbitals did not significantly improve the simulated appearance.
- (69) Gießel, T.; Schaff, O.; Lindsay, R.; Baumgärtel, P.; Polcik, M.; Bradshaw, A. M.; Koebbel, A.; McCabe, T.; Bridge, M.; Lloyd, D. R.; Woodruff, D. P. *J. Chem. Phys.* **1999**, *110*, 9666-9672.
- (70) Haq, S.; King, D. A. *J. Chem. Phys.* **1996**, *100*, 16957-16965.
- (71) Lee, J.-G.; Ahner, J.; Jr, J. T. Y. *J. Chem. Phys.* **2001**, *114*, 1414-1419.
- (72) Demuth, J. E.; Christmann, K.; Sanda, P. N. *Chem. Phys. Lett.* **1980**, *76*, 201-206.
- (73) Bader, M.; Haase, J.; Frank, K.-H.; Puschmann, A.; Otto, A. *Phys. Rev. Lett.* **1986**, *56*, 1921-1924.
- (74) Lin, N.; Dmitriev, A.; Weckesser, J.; Barth, J. V.; Kern, K. *Angew. Chem. Int. Ed.* **2002**, *41*, 4779-4783.

- (75) Messina, P.; Dmitriev, A.; Lin, N.; Spillmann, H.; Abel, M.; Barth, J. V.; Kern, K. *J. Am. Chem. Soc.* **2002**, *124*, 14000-14001.
- (76) Lingenfelder, M.; Spillmann, H.; Dmitriev, A.; Stepanov, S.; Lin, N.; Barth, J. V.; Kern, K. *Chem. Eur. J.* **2004**, *10*, 1913-1919.
- (77) Seitsonen, A. P.; Lingenfelder, M.; Spillmann, H.; Dmitriev, A.; Stepanov, S.; Lin, N.; Kern, K.; Barth, J. V. *J. Am. Chem. Soc.* **2006**, *128*, 5634-5635.
- (78) Crommie, M. F.; Lutz, C. P.; Eigler, D. M. *Science* **1993**, *262*, 218-220.
- (79) Lin, N.; Stepanov, S.; Vidal, F.; Barth, J. V.; Kern, K. *Chem. Commun.* **2005**, 1681-1683.
- (80) Clair, S.; Pons, S.; Brune, H.; Kern, K.; Barth, J. V. *Angew. Chem. Int. Ed.* **2005**, *44*, 7294-7297.



TOC